

Antiferromagnetic Resonance in LaMnO_3 at Low Temperature

Diyar Talbayev and László Mihály

Department of Physics and Astronomy, Stony Brook University, Stony Brook, New York 11794-3800, USA

Jianshi Zhou

Texas Materials Institute, University of Texas, Austin, Texas 78712, USA

(Received 12 November 2003; published 2 July 2004)

The antiferromagnetic resonance modes have been studied on a stoichiometric single crystal of LaMnO_3 well below the Néel temperature, with a static magnetic field along all three crystallographic directions. A canted antiferromagnet model, with biaxial anisotropy and a Dzyaloshinski-Moriya (DM) interaction, explains the results. The DM interaction, often cited as the dominant cause of the canted magnetism, is found to be weak. Instead, the GdFeO_3 -type octahedron rotation leads to the tilted character of the single-ion anisotropy that plays a dominant role in spin canting.

DOI: 10.1103/PhysRevLett.93.017202

PACS numbers: 75.25.+z, 76.50.+g

In an early work Bozorth [1] pointed out a mechanism, based on the asymmetric single-ion anisotropy, for developing weak ferromagnetism in crystals with a strong antiferromagnetic order. Dzyaloshinski and Moriya considered another mechanism, due to the antisymmetric exchange coupling between the two sublattices. Moriya [2] discusses the distinct properties of two prototype canted antiferromagnets, NiF_2 and $\alpha\text{-Fe}_2\text{O}_3$, in terms of single-ion anisotropy and the Dzyaloshinski-Moriya (DM) interaction and shows that the spin wave spectrum responds differently to the two couplings. In the present work we investigate the $\mathbf{k} = 0$ spin waves, detected by antiferromagnetic resonance (AFMR), in stoichiometric LaMnO_3 . Using a recently developed instrument, the AFMR signal was mapped over a wide range of magnetic fields and frequencies on a single crystal oriented in various directions relative to the field. The complete set of parameters responsible for the canted antiferromagnetic (CAF) order has been deduced and discussed in terms of the crystal structure.

The crystal structure and the magnetic structure of LaMnO_3 has been determined in the neutron diffraction studies [3–5]. Below the Néel temperature of $T_N = 141$ K the magnetic order consists of ferromagnetic a - b planes, with the magnetization within the plane either along or opposite the b direction. The order along the c axis is antiferromagnetic. Magnetization studies of Matsumoto [6] on polycrystalline LaMnO_3 samples revealed a weak ferromagnetic moment, which he attributed to the effect of the DM interaction [2,7]. The ferromagnetic moment arises as the spins on the Mn ions tilt out of the a - b plane resulting in the CAF structure and a net magnetization along the c axis. The spin waves in LaMnO_3 have been studied by neutron diffraction by Moussa *et al.* [4], AFMR has been observed by high-field electron spin resonance (ESR) methods by Mitsudo *et al.* [8] and by Pimenov *et al.* [9–11].

The single crystal of LaMnO_3 used in this study was disk shaped, with a diameter of 4 mm and a thickness of

0.6 mm. The directions of the orthorhombic a , b , and c axes with respect to the sample disk were determined by x-ray diffraction. The b axis was found to be perpendicular to disk, the a and c axes are in the plane of the disk. The results of the SQUID magnetization measurements confirming the described orientation of the crystal, as well as the study of magnetic resonance at various temperatures (4.2–250 K) by high-field ESR and fixed-field broad-frequency-band methods, are published elsewhere [12]. The static magnetization and magnetic resonance data [12] suggest that the LaMnO_3 sample is either not twinned or twinned only very slightly.

In the present Letter we report the first complete field-frequency maps of the low temperature ($T = 15, 20$ K) AFMR absorption on a LaMnO_3 single crystal with the static field ranging from 0 to 14 T. The field was oriented along the orthorhombic b axis, as well as in several directions in the a - c plane. AFMR was detected by attenuation of the far-infrared synchrotron radiation passing through the sample, and the frequency content of the transmitted light was analyzed and recorded by an SPS 200 Fourier transform far-infrared spectrometer. The measurement setup, including an Oxford Instruments superconducting magnet, was installed at the National Synchrotron Light Source at the Brookhaven National Laboratory [12]. A room-temperature fluorogold filter was used to limit the high frequency cutoff to 30 cm^{-1} . The lower frequency cutoff was 4 cm^{-1} due to the small size of the apertures. The frequency resolution of 0.5 cm^{-1} was chosen because the AFMR linewidth in our sample is about 1.5 cm^{-1} . Measurements were performed with nonpolarized light incident perpendicular to the sample disk and propagating along the crystallographic b axis. We oriented the static field parallel and perpendicular to the propagation of the light, in the latter case we had the possibility of orienting the field along any direction in the a - c plane.

The raw data are in the form of the transmitted intensity spectra taken at a range of fixed static fields (0–14 T).

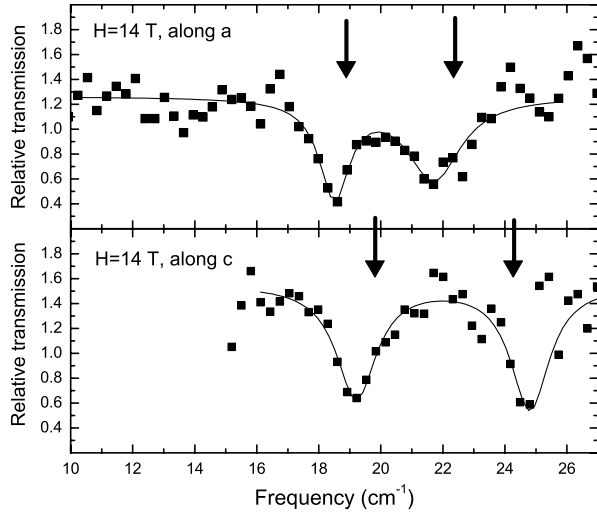


FIG. 1. Relative transmission of the sample with static field along the orthorhombic a and c axes at 14 Tesla. The vertical arrows represent the frequencies calculated using Eqs. (3) and (4).

To analyze the position and shape of the spin resonance lines, background corrections are necessary. These corrections reduce or eliminate intensity variations due to the overall absorption (nonmagnetic in origin) and the multiple reflections within the sample [12]. The end product of the correction procedure is the relative transmission [12] of the sample (Fig. 1); this spectrum shows only the absorption of magnetic resonance origin. After repeating the measurements at several fields we assemble

$$\mathcal{H} = H_e \mathbf{M}_1 \cdot \mathbf{M}_2 / M - D(M_{1b}M_{2c} - M_{1c}M_{2b}) / M - (A_{bb}M_{1b}^2 + A_{cc}M_{1c}^2 + A_{bc}M_{1b}M_{1c}) / M - (A_{bb}M_{2b}^2 + A_{cc}M_{2c}^2 - A_{bc}M_{2b}M_{2c}) / M - \mathbf{H} \cdot (\mathbf{M}_1 + \mathbf{M}_2), \quad (1)$$

where M is the magnitude of \mathbf{M}_1 and \mathbf{M}_2 , and the a , b , and c indices indicate the corresponding vector components. The first two terms describe the exchange and DM interactions, respectively. In the neighborhood of the equilibrium direction the anisotropy energy associated with magnetic moment \mathbf{M}_1 can be expanded into a quadratic expression, its most general form is given by the third term in (1). This form of anisotropy energy corresponds to the easy axis in the b - c

the relative transmission spectra into field-frequency maps where the darker shade of gray corresponds to the stronger absorption (Fig. 2).

We recorded AFMR spectra with the static field along all three orthorhombic axes. In the a - c plane we oriented the field along the a axis, along the c axis, and at 45° angle between the a and c axes. The spectra with the static field along the a axis at 0 and 14 Tesla are shown in Fig. 1. Field-frequency maps in Fig. 2 show the field dependence of the resonance frequencies when the static field is along c axis, when it makes a 45° angle with the c axis, and when the static field is along the b axis. In all cases the zero field resonance is split into two modes in finite external field.

A model of a canted two-sublattice antiferromagnet explains the observed resonance frequency dependence on the direction and magnitude of the external field. Skumryev [13] *et al.* measured the weak ferromagnetic moment in LaMnO_3 along the c axis to be $M_c = 0.18 \mu_B/\text{Mn}$ in the absence of the external field and concluded that both DM exchange and crystal field anisotropy are necessary to explain the CAF order. Moriya [2] discussed the influence of the anisotropy and DM interaction separately; Herrmann [14] calculated the field dependence of spin resonance frequencies in CAF substances with both interactions present. Our discussion is based on the latter calculation.

We consider our CAF structure to be composed of two sublattices carrying magnetic moments \mathbf{M}_1 and \mathbf{M}_2 . The energy of the system is given by

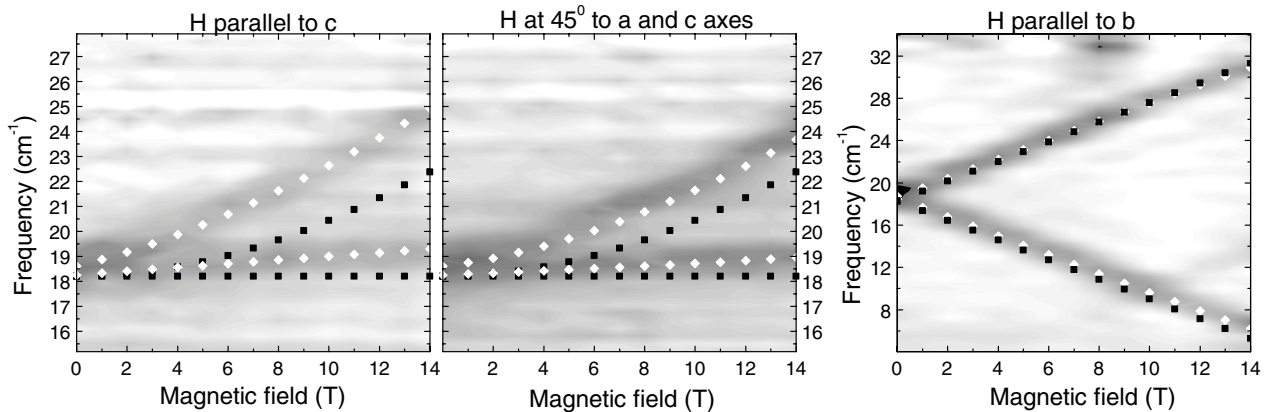


FIG. 2. Frequency-field dependence of AFMR with static field in the a - c plane and along the b axis. Black squares represent the frequencies calculated according to Kittel's theory. White diamonds on the left and right indicate the frequencies calculated using Herrmann's [14] formulas. White diamonds in the middle are the linear interpolation between calculated frequencies for $H \parallel c$ and $H \parallel a$.

plane making an angle θ with the b axis, so that $\tan 2\theta = A_{bc}/(A_{bb} - A_{cc})$. A rotation of the reference frame by θ diagonalizes the anisotropy energy tensor. Because of the mirror planes at $1/4$ and $3/4$ positions in the c direction, the angle must alternate between θ and $-\theta$ for subsequent planes (located at 0 , $1/2$, and 1 in the unit cell; numbers are in units of c lattice parameter), leading to the opposite signs of the $A_{bc}M_bM_c$ terms for \mathbf{M}_1 and \mathbf{M}_2 in Eq. (1). The exchange, DM, and anisotropy constants are in the units of magnetic field. Solving the equations of motion of the sublattices, we get the following resonance frequencies [14]: for $\mathbf{H} = 0$,

$$\omega_1^2(0)/\gamma^2 = 4H_e(A_{bb} - A_{cc}) + 4A_{bb}(A_{bb} - A_{cc}) + 4A_{bc}(A_{bc} + D), \quad (2a)$$

$$\omega_2^2(0)/\gamma^2 = 4H_eA_{bb} + 4A_{bb}(A_{bb} - A_{cc}) + (A_{bc} + D)^2, \quad (2b)$$

for \mathbf{H} in c direction,

$$\omega_1^2/\gamma^2 = \omega_1^2(0)/\gamma^2 + (5A_{bc} + D)H + H^2, \quad (3a)$$

$$\omega_2^2/\gamma^2 = \omega_2^2(0)/\gamma^2 + (A_{bc} + D)H, \quad (3b)$$

and for \mathbf{H} in a direction,

$$\omega_1^2/\gamma^2 = \omega_1^2(0)/\gamma^2 - \frac{4A_{bc}^2}{4A_{cc}H_e + (D + A_{bc})(D - 3A_{bc})}H^2, \quad (4a)$$

$$\omega_2^2/\gamma^2 = \omega_2^2(0)/\gamma^2 + \frac{4A_{cc}H_e + (D - A_{bc})^2}{4A_{cc}H_e + (D + A_{bc})(D - 3A_{bc})}H^2. \quad (4b)$$

Here $\gamma = g\mu_B/\hbar$ is the gyromagnetic ratio. If we take the constants A_{cc} , A_{bc} , and D to be 0, Eqs. (2)–(4) take the form of AFMR frequencies found by Kittel [15] for \mathbf{H} perpendicular to the easy axis,

$$\omega_1 = \gamma\sqrt{H_a(H_a + 2H_e) + H^2}, \quad (5a)$$

$$\omega_2 = \gamma\sqrt{H_a(H_a + 2H_e)}. \quad (5b)$$

The phenomenological anisotropy field is $H_a = 2A_{bb}$.

We used Eqs. (2)–(4) to fit four variables D , A_{bb} , A_{bc} , and A_{cc} assuming fixed $H_e = 33.9$ T [8]. We looked for the best match of the resonance frequencies with static field H between 6 and 14 T along c , $H = 14$ T along a , and $H = 0$ T. A least squares fit of the measured and calculated frequencies yields $D = 1.2$, $A_{bb} = 2.6$, $A_{bc} = 1.6$, $A_{cc} = -0.01$ T. Frequencies calculated using these constants are shown by white diamonds on Fig. 2 and by vertical arrows on Fig. 1. The corresponding reduced χ^2_ν , a quality-of-fit measure, is 1.3. We attempted to fit our data using the model of Pimenov *et al.* [9], which is equivalent to our model with $A_{bc} = A_{cc} = 0$. The minimization of χ^2_ν yields $\chi^2_\nu = 25$, and the calculated frequencies exhibit systematic deviations from the measured frequencies. The difference in the quality of fits with and

without the staggered anisotropy convinces us that the parameter A_{bc} is indispensable in explaining our data. Although Eqs. (2) predict a splitting in the zero-field frequency, our spectra at zero field show a single resonance line at 18.5 cm $^{-1}$ due to the splitting being considerably smaller than the linewidth. For comparison, black squares on Fig. 2 show the resonance frequencies of a uniaxial antiferromagnet calculated using Eqs. (5). Our value of $A_{bb} = 2.6$ T agrees well with $H_a = 2A_{bb} = 5.3$ T found by Mitsudo [8]. The DM constant $D = 1.2$ T can be compared with Mitsudo's 0.2 T and with $D = 2.2$ T deduced from Skumryev's [13] static magnetization measurements.

Expressions similar to Eqs. (2)–(4) can be derived for resonance frequencies with static field along b axis as well. White diamonds in the right panel of Fig. 2 represent the calculated frequencies, while the black squares show the frequencies calculated using Kittel's [15] formula when the static field is along the easy axis

$$\omega_{1,2} = \gamma\sqrt{H_a(H_a + 2H_e)} \pm \gamma H. \quad (6)$$

The effect of the CAF structure on resonance frequencies is barely noticeable.

The angle θ between the easy axis of \mathbf{M}_1 and the b direction is $\theta = 16^\circ$, and the components of the diagonal anisotropy tensor in the rotated reference frame are $A'_{bb} = 2.8$ and $A'_{cc} = -0.2$ T. (The negative A'_{cc} means that the magnetization can be slanted towards a more easily than towards c .) The equilibrium orientation of sublattice magnetizations in the b - c plane in zero static field is given by [14] $\tan 2\alpha_0 = (A_{bc} + D)/(H_e + A_{bb} - A_{cc})$, where α_0 is the angle between \mathbf{M}_1 and the b axis. This relation shows that no canting is possible when both $A_{bc} = 0$ and $D = 0$. The canting angle deduced from our parameter values is $\alpha_0 = 2.2^\circ$. The corresponding 0.16 μ_B/Mn spontaneous magnetization in the c direction is in good agreement with the magnetization measured by Skumryev [13] and consistent with our own magnetization measurements [12].

Why is the easy axis tilted by 16° out of the a - b plane of the crystal? The available crystallographic information [5] and the electronic structure of the Mn^{3+} ion provide a nontrivial answer. The diagonals of the MnO_6 octahedra are not equal, partly due to the Jahn-Teller transition that happens around 800 K. If there were no other distortions, the occupied e_g orbitals would lie in the a - b plane, arranged in an alternating “checkerboard” fashion, so that the angle between the main axis of the occupied e_g orbital and the b direction is either $+45^\circ$ or -45° . The spin-orbit coupling results in a uniaxial magnetic anisotropy: on each Mn the local easy axis is along the axis of the e_g orbital. In this sense the sublattice magnetizations \mathbf{M}_1 and \mathbf{M}_2 are each composed of two subsublattices: $\mathbf{M} = \mathbf{M}^+ + \mathbf{M}^-$ ($\mathbf{M} = \mathbf{M}_1$ or \mathbf{M}_2) corresponding to spins with two different anisotropy directions. The ferromagnetic exchange [4] is much

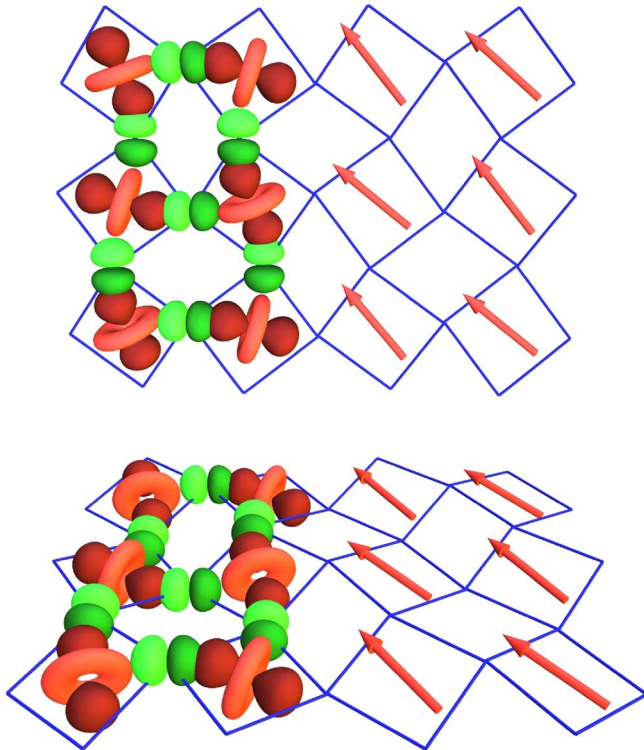


FIG. 3 (color online). Basal planes of the MnO_6 octahedra are represented by squares. A view along the c axis is on the top, a view along a direction approximately 45° with the b axis is at the bottom. The Mn ions are in the center of the square, oxygens are at the vertices. The left part of the figure illustrates the occupied e_g orbitals and the relevant p orbitals of oxygen; the arrows on the right represent the spins. For a fully three-dimensional view see our website [16].

stronger than the single-ion anisotropy energy. Therefore, \mathbf{M}^+ and \mathbf{M}^- will be parallel. The anisotropy of \mathbf{M} becomes planar, because the anisotropies of \mathbf{M}^+ and \mathbf{M}^- are uniaxial with 90° angle between the axes.

To understand the uniaxial anisotropy energy of \mathbf{M}_1 (or \mathbf{M}_2), we consider the basal plane of each MnO_6 octahedron, defined as the plane where the occupied e_g orbital lies, makes a nonzero angle to the a - b plane (Fig. 3). The rotation of each octahedron by $\pm 15^\circ$ around a selected $[111]$ direction of the pseudocubic unit cell [5] leads to a tilt that results in $\pm 35^\circ$ angle between the easy magnetization axes of \mathbf{M}^+ and \mathbf{M}^- and the b direction. Therefore moments select b (as opposed to a) when the ferromagnetic coupling is introduced.

It is natural (but wrong) to assume that the local easy axis of each Mn spin is along the diagonal of the MnO_6 octahedron. The diagonal makes a 8° angle to the a - b plane; the easy axis of $\mathbf{M} = \mathbf{M}^+ + \mathbf{M}^-$ would be about 10° , but still too small compared to the observed 16° . The discrepancy can be resolved, at least qualitatively, once we consider the “finite size” and “rigidity” of the electronic orbitals. The rotation of the octahedron was derived from the position of the oxygen nuclei, but the

single-ion anisotropy is related to the orientation of the Mn e_g orbitals. The orbitals do not reach the oxygen nuclei, but overlap with the p orbitals of the oxygens. As a result, when the octahedra tilt, the occupied e_g orbitals inevitably turn *more* than the octahedra, as the left side of Fig. 3 illustrates. Naturally, the larger tilt angle of the orbitals leads to the larger tilt angle of the easy axis.

In conclusion, we deduced the anisotropy field ($2A'_{bb} = 5.6$ T) and the DM coupling constant ($D = 1.2$ T) from AFMR measurements on LaMnO_3 . We find that the main cause of the canted magnetism is the tilted nature of the easy axis, alternating $\pm 16^\circ$ relative to the a - b plane. The calculated value of the moment agrees well with the measured one, and the crystal structure offers a reasonable explanation for the observed anisotropy.

Valuable discussions with P.B. Allen, A. Janossy, and G.L. Carr are acknowledged. This work was supported by the National Science Foundation (DMR 0132282), and by DARPA/UCLA (1000GCG008). The work at the Nation Synchrotron Light Source is supported by the Department of Energy, under Contract No. DE-AC02-98CH10886.

- [1] R. M. Bozorth, Phys. Rev. Lett. **1**, 362 (1958).
- [2] T. Moriya, in *Magnetism*, edited by G.T. Rado and H. Suhl (Academic Press, New York, 1984), Vol. I, p. 85.
- [3] E. O. Wollan and W.C. Koehler, Phys. Rev. **100**, 545 (1955).
- [4] F. Moussa, M. Hennion, J. Rodriguez-Carvajal, H. Moudden, L. Pinsard, and A. Revcolevschi, Phys. Rev. B **54**, 15 149 (1996).
- [5] J. Rodriguez-Carvajal, M. Hennion, F. Moussa, A. H. Moudden, L. Pinsard, and A. Revcolevschi, Phys. Rev. B **57**, R3189 (1998).
- [6] G. Matsumoto, J. Phys. Soc. Jpn. **29**, 606 (1970).
- [7] I. Dzyaloshinski, J. Phys. Chem. Solids **4**, 241 (1958).
- [8] S. Mitsudo, K. Hirano, H. Nojiri, M. Motokawa, K. Hirota, A. Nishizawa, N. Kaneko, and Y. Endoh, J. Magn. Magn. Mater. **177–181**, 877 (1998).
- [9] A. Pimenov, M. Biberacher, D. Ivannikov, A. Loidl, V. Y. Ivanov, A. A. Mukhin, and A. M. Balbashov, Phys. Rev. B **62**, 5685 (2000).
- [10] A. A. Mukhin, V.Y. Ivanov, V.D. Travkin, A. Pimenov, A. Loidl, and A. M. Balbashov, Europhys. Lett. **49**, 514 (2000).
- [11] D. Ivannikov, M. Biberacher, H.-A. K. von Nidda, A. Pimenov, A. Loidl, A. A. Mukhin, and A. M. Balbashov, Phys. Rev. B **65**, 214422 (2002).
- [12] L. Mihaly, D. Talbayev, L. F. Kiss, J. Zhou, T. Fehér, and A. Jánossy (to be published).
- [13] V. Skumryev, F. Ott, J.M.D. Coey, A. Anane, J.-P. Renard, L. Pinsard-Gaudart, and A. Revcolevschi, Eur. Phys. J. B **11**, 401 (1999).
- [14] G. F. Herrmann, J. Phys. Chem. Solids **24**, 597 (1963).
- [15] F. Keffer and C. Kittel, Phys. Rev. **85**, 329 (1952).
- [16] <http://infrared.physics.sunysb.edu/LaMnO3>